Lin *et al. Advances in Bridge Engineering* (2026) 7:12
https://doi.org/10.1186/s43251-026-00204-9

Advances in
Bridge Engineering

ORIGINAL INNOVATION Open Access

Modelling the effect of the water evaporation rate on total shrinkage of blended cement concrete

Htet Nyi Nyi Lin[1], Quang Dieu Nguyen[1*] and Arnaud Castel[1]

*Correspondence:
quangdieu.nguyen@uts.edu.au

[1] School of Civil
and Environmental Engineering,
University of Technology Sydney
(UTS), Sydney, NSW 2007,
Australia

Abstract

Concrete shrinkage is a key factor affecting the serviceability and durability of bridge structures, particularly in elements such as decks, girders, and piers where restrained shrinkage can lead to cracking and long-term performance issues. The incorporation of supplementary cementitious materials (SCMs), such as fly ash and ground granulated blast furnace slag (GGBFS), significantly influences shrinkage behaviour. In addition, environmental conditions commonly encountered on bridge construction sites—such as elevated temperature, low relative humidity, and wind—can accelerate moisture loss, increasing the risk of shrinkage-induced cracking. This study investigates the total shrinkage of nine concrete mixes with 28-day compressive strengths ranging from 30 to 70 MPa, incorporating binder compositions of 30% fly ash, 40% slag, and 60% slag. Specimens were exposed to controlled environmental conditions to quantify the effects of temperature, humidity, and wind on shrinkage development. Based on experimental results, a new predictive model is proposed to estimate total shrinkage under harsh "field conditions" from shrinkage measured or calculated under standard laboratory conditions (23°C and 50% relative humidity). The results indicate that shrinkage under harsh conditions initially increases to a peak before gradually converging to standard-condition values at a defined "merging time." While binder composition had only a marginal effect on this trend, compressive strength significantly influenced the merging time, which increased with higher strength levels. The proposed model demonstrates excellent predictive capability for concretes with compressive strengths between 30 and 70 MPa, including mixes with 100% general-purpose cement and SCM-blended binders. These findings provide a practical tool for bridge engineers to account for environmental effects on shrinkage, improving serviceability design and reducing the risk of early-age cracking in bridge structures.

Keywords: Shrinkage, Concrete, Fly ash, GGBFS, Wind speed, Water evaporation rate

1 Introduction

Serviceability is a fundamental requirement in concrete bridge structures, where controlling deformation and cracking is essential for long-term durability and performance. Among the factors influencing serviceability, concrete shrinkage is particularly critical because it affects volume stability and early-age cracking in structural components

Springer

such as bridge decks, girders, piers, and abutments. Shrinkage-induced cracking can compromise structural integrity, reduce durability, and accelerate maintenance needs. Numerous models have been developed to incorporate shrinkage effects in serviceability design for reinforced concrete slabs, columns, and composite bridge decks (Gilbert et al. 2012; Ma et al. 2025; Dhahir and Marx 2024; Choudhary et al. 2021; Aziz et al. 2022; Bisht and Ramana 2022; Hui et al. 2024). However, regardless how complex models are, serviceability design can be successful only if concrete shrinkage itself can be accurately estimated by accounting for the field environmental conditions. This is particularly important at early age when the concrete tensile strength is low, and the risk of restrained shrinkage induced cracking is high.

As Portland cement production is a major source of carbon dioxide emissions, researchers are looking for solutions allowing to reduce the carbon emissions of the construction industry (John et al. 2019). One of the possible solutions is the use of supplementary cementitious materials (SCMs) such as fly ash or Ground Granulated Blast Furnace Slag (GGBFS) as a partial replacement of cement in concrete. These SCMs are by-products from other industries such as coal-fired power plants for fly ash or steel manufacture for GGBFS. As a result, using SCMs in concrete reduces the emissions of CO_2 and allows to recycle wastes from other industries (Giergiczny 2019). Although SCMs tend to have cement-like properties, they still differ significantly in term of chemical composition and reactivity compared to Portland cement, impacting both blended cement hydration and concrete microstructure. As a result, concrete shrinkage is impacted by SCMs (Brooks and Johari 2001; Gedam et al. 2016; Zhang et al. 2023a; Nguyen et al. 2022) as shrinkage occurs by self-desiccation processes related to cement hydration or due to the evaporation of internal moisture to the environment governed by the nature of the pores network of concrete. Among the various SCMs, fly ash and GGBFS are the most commonly used in bridge construction; therefore, this study focuses on their impact on shrinkage in blended cement concretes.

Shrinkage in hardened concrete is normally categorized as autogenous shrinkage and drying shrinkage (Gilbert and Ranzi 2010). Drying shrinkage is due to the loss of concrete internal moisture to the environment by evaporation. Autogenous shrinkage occurs due to the so-called self-desiccation process of concrete and is not related to any moisture evaporation. Many factors influence both types of shrinkage and were extensively investigated, including binder composition, water to cement ratio, effect of curing duration and conditions etc. (Zhang et al., 2023a; Nguyen et al., 2022; Afroz et al., 2023; Asamoto et al., 2023; Chu et al., 2012; Lura et al., 2001; Piasta & Zarzycki, 2017; Sakata & Ayano, 2000; Zhang et al., 2013; Afroz et al., 2022). The environmental temperature and relative humidity are also critical factors that can increase shrinkage by accelerating the internal water evaporation. While predicting concrete total shrinkage, wind is also one of the environmental factors to consider as it can accelerate the moisture evaporation from the concrete. Studies considering the influence of combined environmental factors such as temperature and relative humidity and wind on the shrinkage of concrete are still very limited (Barluenga et al. 2018; Yalçınkaya and Yazıcı 2017). No studies are attempting to quantify and model this environmental impact on total shrinkage of concrete, particularly at early age.

Standard models have been developed all around the world aiming to predict the time-dependent total shrinkage of concrete including the effects of concrete mix composition, compressive strength, environmental conditions etc. However, Standard model codes were calibrated to predict the final shrinkage strain of concrete, sometime named design shrinkage strain. As a result, design codes focus primarily on long term shrinkage and not on early age shrinkage. Environmental conditions such as relative humidity and temperature can greatly influence early age shrinkage which is not adequately captured by standard models. For example, in Australian Standard AS3600, a parameter accounts for the effects of humidity and temperature associated with different environments and equals 0.70 for arid environments, 0.65 for interior environments, 0.60 for temperate environments and 0.50 for tropical and coastal environments. As a result, at all age, the difference in shrinkage between interior environment (about 20 °C and 50–60% relative humidity) and arid conditions is less than 10%. In this paper, concrete total shrinkage measured in standard conditions (23 °C and 50% relative humidity) was compared to the shrinkage of similar concrete specimens stored in harsh arid conditions (38 °C and 20% relative humidity). After 7 days of exposure, shrinkage in harsh arid condition was about twice the shrinkage measured in standard conditions, demonstrating that Standard model codes cannot capture adequately the effect of environmental conditions on early age concrete shrinkage. Another evidence is that, in all standard design codes, the effect of temperature and relative humidity is not time-dependent. This means that the values of the factors or functions used to capture environmental effects are the same at early age and at long term. However, all experimental results reported in this paper, showing that shrinkage greatly increased at early age in harsh environment, also show that concrete shrinkage of specimens exposed to standard conditions or harsh arid conditions become similar after some time, so-called merging-time. This is a clear shortcoming of the current models. To address this gap, a new time-dependent shrinkage factor, labelled Sh(wer, t) is introduced. Sh(wer, t) is capturing the effect of the water evaporation rate in the field (wer) calculated based on the environmental temperature and relative humidity. The effect of the water evaporation rate on shrinkage is strong at early age but fades after the so-called merging-time is reached. This new time-dependent shrinkage factor will enable bridge engineers to better predict shrinkage under site-specific conditions, particularly at early ages when the risk of cracking is the greatest.

Importantly, Sh(wer,t) is a correction factor to existing models allowing to capture the effects of environmental temperature and relative humidity on early age shrinkage. Sh(wer,t) does not change model's predictions of long-term shrinkage as Sh(wer,t) is equal to 1 after the merging-time is reached. In this paper, for calibration purpose, the concrete shrinkage measured experimentally in Australian Standard AS1012.13 standard conditions (23 °C temperature and 50% relative humidity) is multiplied by Sh(wer,t) to fit the shrinkage values measured experimentally in harsh conditions.

At the construction site, freshly poured concrete may be exposed to hot and windy conditions. This situation may cause the freshly placed concrete to crack during its plastic stage, so-called, plastic shrinkage induced cracking (Uno 1998). But, in this study, concrete plastic shrinkage will not be considered. The work focuses only on total shrinkage of hardened concrete.

In this study, concretes with 28-day compressive strengths ranging from 30 to 70 MPa are considered with different percentages of SCMs including 30% fly ash, 40% Slag and 60% Slag. Only the concrete total shrinkage is investigated. The shrinkage behaviour of blended cement-based concretes is compared to that of a reference concrete with 100% general purpose cement for each concrete compressive strength.

2 Experimental program

2.1 Materials and concrete mix designs

The binders considered in this study include General Purpose (GP) cement, fly ash (FA) and Slag (SL). The GP cement complied with AS 3972 (AS, As 3972 2010). The commercial name of the FA and SL, supplied by Boral, is Blue Circle Fly Ash and Environment® respectively, also known as Ground Granulated Blast Furnace Slag. In addition, the chemical composition of the GP Cement, Fly Ash (FA) and Ground Granulated Blast furnace slag (SL) was analysed using the wavelength-dispersive X-ray fluorescence (WDXRF) technique. The results obtained from XRF analysis are provided in the Table 1.

The aggregates used in this study for mix designs are Sydney Sand as fine aggregates and 10 mm Basalt as coarse aggregates. While the Sydney sand has the specific gravity of 2.65 and water absorption 3.5%, the basalt coarse aggregates had 2.80 and 1.08% respectively. The 10 mm basalt was selected as coarse aggregate is because the study from Jin et al. (Jin et al. 2020) had proved that 10 mm aggregates are better to batch and fit well in small spaces, such as shrinkage moulds, than 20 mm aggregates.

In this study, 9 concrete mixes were considered. The detailed proportions of the mix designs are presented in Table 2. To assure that concrete blended with fly ash or slag are achieving similar compressive strength with reference concrete (100% GP cement), the water binder ratio was adjusted through trial mixes.

The concrete mixes were divided into three grades achieving an average 28-day compressive strength of about 32 MPa, 45 MPa and 65 MPa, covering a wide range of applications. Each concrete grade has a reference concrete mix which does not include any SCM, labelled either C32-0, C45-0 or C65-0. As for the blended cement concrete mixes, either 30% of fly ash or 40% Slag or 60% Slag as partial replacement of GP cement were

Table 1 Chemical Composition of GP cement and SCMs

Materials	GP cement (wt%)	Fly ash (wt%)	GGBFS (wt%)
CaO	64.1	1.3	42.8
SiO_2	19.1	62.5	35.6
Al_2O_3	5.4	25.2	13.5
Fe_2O_3	2.9	4.6	0.1
SO_3	3.0	< 0.1	0.6
MgO	1.1	0.6	5.8
Na_2O	0.2	0.4	0.2
K_2O	0.6	1.5	0.4
P_2O_5	< 0.1	0.3	< 0.1
Loss on ignition (LOI)	3.6	1.7	0.1

Table 2 Mix design of concretes

			Mix Proportions by Weights (kg/m^3)						
Mix Type	**FA%**	**GGBFS%**	**GPC**	**FA**	**GGBFS**	**CoA**	**FiA**	**SP (ml/m^3)**	**w/b**
C32-0	0	0	310	0	0	1059	866	430	0.56
C45-0	0	0	360	0	0	1025	839	500	0.49
C45-FA30	30	0	250	110	0	1043	853	500	0.40
C45-G40	0	40	215	0	145	1033	845	500	0.45
C45-G60	0	60	145	0	215	1037	848	500	0.43
C65-0	0	0	510	0	0	927	759	700	0.40
C65-FA30	30	0	355	155	0	955	782	700	0.30
C65-G40	0	40	305	0	205	930	761	700	0.39
C65-G60	0	60	205	0	305	941	770	700	0.35

* *FA* fly ash, *GGBFS* ground granulated blast furnace slag, *GPC* General Purpose Cement, *CoA* Coarse aggregate, *FiA* Fine Aggregate, *SP* Superplasticiser, *w/b* water/binder ratio

included as outlined in Table 2. For grade 32 MPa concrete, no blended cement concrete mixes were included, only the reference mix (Table 2).

Before mixing, all aggregates are in saturated surface dry (SSD) condition to ensure that there will be no excess water or absorbed in the aggregates which can impact the water to binder (w/b) ratio. During the batching of the concrete, SSD condition aggregates were dry mixed for 2 min, followed by 5 more minutes after adding both binder and water. To maintain the workability, superplasticizer was added during the mixing and the type of the superplasticizer used was Polycarboxylic Ether Polymer, MasterGlenium SKY 8100. When the mixing is complete, the concrete is put into the moulds. The moulds consist of steel prisms for shrinkage measurement and steel cylinder moulds for compressive strength testing. The size of the cylindrical steel moulds is 100 mm diameter by 200 mm height. Shrinkage specimens are $75 \times 75 \times 280$ mm prisms.

2.2 Concrete compressive strength test

After batching, concrete is poured into 3 cylindrical moulds. The top of the moulds is sealed with a steel cap to avoid any water evaporation. Concrete is then left in the cylinder for 1 day to set and harden. After 24 h, the cylindrical concrete specimens were taken out of the moulds and transferred into a curing tank and stored in water for 7 days. Then, the cylinder specimens were taken out of the curing tank and transferred into a controlled room consisting of a temperature 23 °C and a relative humidity (RH) of 50% until 28-day. The 28-day compressive strength was measured using a UTEST testing equipment with the loading rate of 20 MPa per minute complying with ASTM C39 (ASTM 2018). Three specimens were tested to calculate the average 28-day compressive strength and the standard deviation.

2.3 Concrete total shrinkage tests

In this study, only the total shrinkage of concrete is measured. Total shrinkage monitoring starts 24 h after casting the specimens while concrete is hardening. As mentioned before, plastic shrinkage is excluded from this study. Two controlled rooms with different temperature and relative humidity are used to examine the impact of environmental factors including temperature, humidity, and wind speed on concrete total shrinkage.

One room produces severe environmental conditions, maintaining a temperature of 38 °C and a relative humidity of 20%. The temperature of 38 °C was chosen for this study as it is representative of Australian severe summer conditions with high temperature and low humidity. The second controlled room provides standard testing conditions for concrete shrinkage as per Australian Standard AS1012.13, with a temperature of 23 °C and a relative humidity of 50%.

Additionally, fans were placed in front of some prisms in the 38 °C temperature room to investigate the effect of wind on concrete total shrinkage as shown in Fig. 1. These fans can generate wind speeds ranging from 10 to 24 km/h.

In 1998, Paul Uno (Uno 1998) developed a "single operation" model (Eq. (1)) that can predict the rate of evaporation from the concrete surface based upon the Menzel's formula.

$$\text{wer} = 5\left([T_c + 18]^{2.5} - r\,[T_a + 18]^{2.5}\right)(V + 4) \times 10^{-6} \quad (1)$$

Where wer is the water evaporation rate in kg/m^2/hr, T_C is the concrete (water surface) temperature in degrees Celsius, T_a is the air temperature in degrees Celsius, r is the relative humidity (percent)/100 and V is the wind velocity in kph. From Eq. (1), the evaporation rate (wer) in standard conditions (temperature of 23^{0}C, relative humidity of 50% and no wind) is calculated as 0.11 kg/m^2/hr when the concrete temperature is assumed to be the same as the air temperature. Adding the effect of a wind speed of 20 kph, the evaporation rate would be increased to 0.65 kg/m^2/hr, leading to a wer about six-time higher than in standard conditions. In comparison, the water evaporation rate calculated without wind but with a temperature of 38^{0}C and relative humidity (RH) of 20% is equal to only 0.375 kg/m^2/hr. As result, even if the maximum wind speed delivered by the fan of 24 kph seems low, its effect on the wer is greater than that of the humidity and temperature conditions in the 38^{0}C room according to Eq. (1). Therefore, in this study, wind speeds ranging from 10 to 25 kph are used and considered suitable to assess the effect of wind on hardened concrete total shrinkage.

24 h after batching, all concrete prisms (9 in total per concrete mix design) were demoulded. Three of them were stored in the 23^{0}C standard room and the other six were stored in the 38^{0}C room. In the 38^{0}C room, 3 prisms were exposed to the fan action and 3 prisms were not, allowing to estimate the effect of the wind speed on concrete total shrinkage. While placing prisms in each room, it was ensured that all the surfaces of the

Fig. 1 38 °C and 20% R.H. controlled room including wind action

concrete were not being covered by any materials nor being close to the rooms walls which could interfere with the shrinkage development. As the next step, the measurements of the specimen are carried out once a day for first 7 days including the initial measurements, then twice a week until specimens reach the age of 14 days, and then once a week until the specimens reached the age of 30 days and once a month until shrinkage development becomes negligible.

To account for the 15 °C difference in temperature between the two controlled rooms, the concrete thermal expansion was considered when calculating the shrinkage values in the 38 °C room. A concrete coefficient of thermal expansion (CTE) of 10 microstrain/°C was selected in accordance with the Eurocode 2 recommendations for concrete with Basalt as coarse aggregate (EN 2015). Since there was 15 ^{0}C difference, 150 microstrains were added to the shrinkage measured in harsh condition (38 ^{0}C and relative humidity of 20%) to account for the thermal expansion of concrete. Although blended cement concretes, particularly slag blends, may exhibit slightly lower thermal expansion due to their refined pore structure (Zhang et al. 2023b), a previous study showed that CTE is primarily governed by aggregate type, which represents about 70% of concrete volume, while binder composition has only a secondary influence (Meyers 1951). Reported ranges for CTE in normal-weight concretes are typically 7–13 microstrain/°C, with most values fluctuating around 10–11 microstrain/°C regardless of SCM content (EN 2015). Therefore, applying a uniform correction based on 10 microstrain/°C is appropriate for isolating shrinkage behaviour under different temperature conditions.

3 Results and discussion

3.1 Compressive strength of concrete

The 28-day average compressive strength of the concretes is presented in Table 3 including the standard deviation.

3.2 Total shrinkage of concrete

Figure 2 shows the total shrinkage of C45-0, C45-F30, C45-G40, and C45-G60 concretes, measured in the 23^{0}C and 38^{0}C rooms for about 4 months. At early age, due to the higher water evaporation rate, the total shrinkage of concrete specimens exposed

Table 3 Concrete 28-days average compressive strength

Concrete	Average 28-day Compressive Strength (MPa)
C32-0	32.8 ± 0.9
C45-0	43.6 ± 2.2
C45-FA30	41.5 ± 0.6
C45-G40	47.6 ± 1.4
C45-G60	43.1 ± 1.2
C65-0	69.7 ± 0.6
C65-FA30	71.0 ± 1.0
C65-G40	67.3 ± 0.1
C65-G60	66.7 ± 0.6

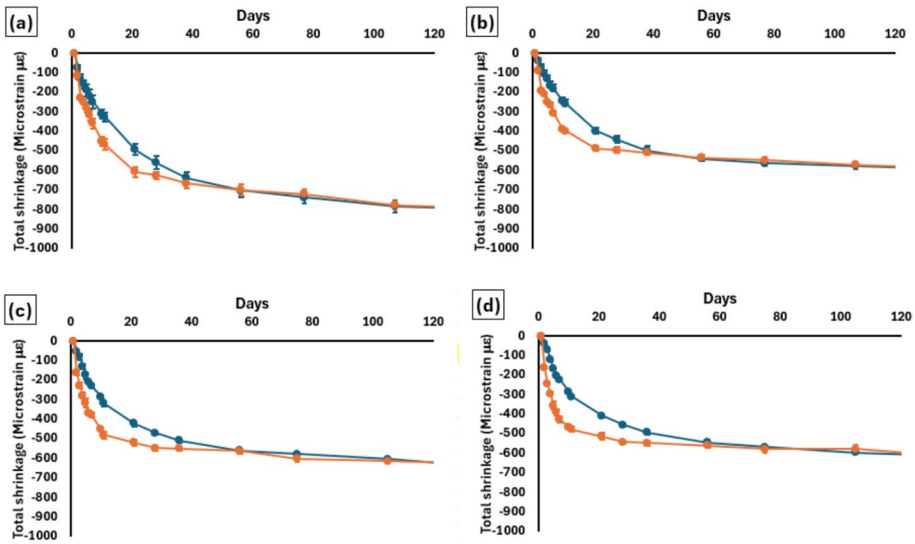

Fig. 2 Total Shrinkage of (**a**)C45-0, (**b**)C45-F30, (**c**)C45-G40, (**d**)C45-G60 in both 23^0C and 38^0C rooms

to the 38^0C environment is notably higher than that of specimens stored in standard conditions (temperature 23 °C and RH of 50%).

However, after about two weeks, the total shrinkage development rate of the concrete specimens exposed to the 38^0C environment tends to reduce significantly. After about 40 to 60 days, the total shrinkage values of concretes exposed to the 38^0C environment become similar to those of concretes exposed to the 23 °C environment. Furthermore, the total shrinkage of the specimens placed in the 38^0C environment tends to stabilize earlier than for specimens exposed to standard conditions. It appears that the long-term total shrinkage of concrete, often called final shrinkage strain in design Standards, seems not to be dependent on the environmental exposure. In other words, accounting for climatic zones (environmental exposure conditions of the structures) in design Standards might not necessarily be needed for predicting the final concrete total shrinkage strain.

Furthermore, the results indicate that fly ash and GGBFS contribute to a reduction in total shrinkage of concrete. For example, at 75-day, the total shrinkage strain of C45-0 is over 700 microstrains while the total shrinkage strains of the C45 Concretes with fly ash or slag range between 500 to 600 microstrains.

Figure 3 shows the total shrinkage development concretes C65-0, C65-F30, C65-G40, and C65-G60, measured in the 23^0C and 38^0C rooms for about 4 months. Like C45 concretes, the rate of total shrinkage of concrete specimens exposed to the 38^0C environment is higher at early age. However, at long term, the total shrinkage values of concrete exposed to the 23 °C and the 38^0C environments also become similar. One noteworthy difference between 45 MPa concretes and 65 MPa concretes is the longer time required for shrinkage values to merge, being 80 to 100 days for the 65 MPa concretes. Figures 2 and 3 results also suggest that the binder composition has no significant influence on the time required for 23^0C and 38^0C shrinkages to merge. Finally, as observed for the 45 MPa concretes, fly ash and GGBFS contribute to a reduction

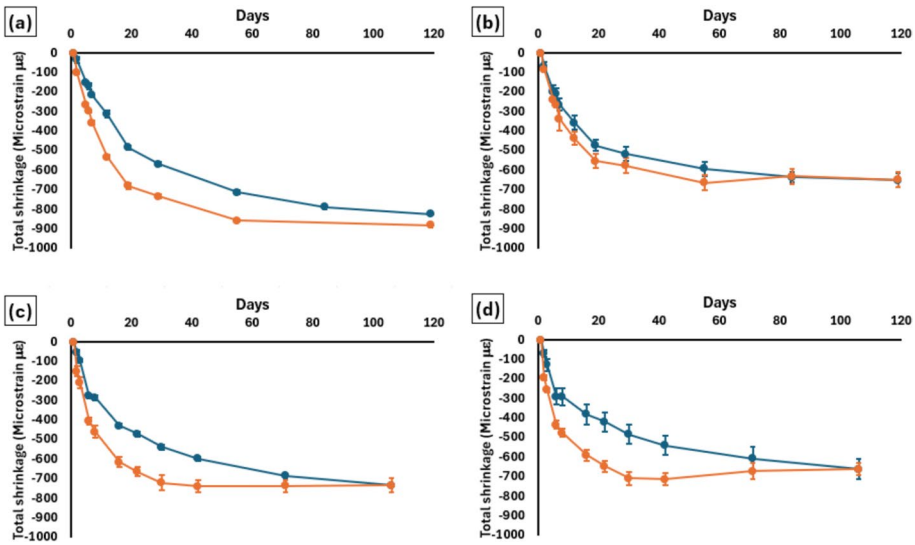

Fig. 3 Total Shrinkage of (**a**)C65-0, (**b**)C65-F30, (**c**)C65-G40, (**d**)C65-G60 in both 23^0C and 38^0C rooms

in total shrinkage of 65 MPa concretes. The reduction in total shrinkage for fly ash and slag concretes can be explained by their secondary hydration mechanisms and resulting pore refinement. Fly ash exhibits pozzolanic activity, reacting with calcium hydroxide during cement hydration to form additional C-S–H with a lower Ca/Si ratio. The pozzolanic reaction, prominent after 14 days, fills capillary pores and results in reducing porosity and permeability. Slag demonstrates latent hydraulic properties, reacting to produce C-S–H and hydrotalcite-type phases in cement paste that significantly refine the pore structure and increase tortuosity (Giergiczny 2019; Snellings et al. 2012). This pore refinement limit internal moisture diffusion, thereby reducing shrinkage. Consequently, concretes with high content of fly ash and slag exhibit lower shrinkage than plain Portland cement concrete mixes, which is consistent with previous studies (Atiş 2003; Dellinghausen et al. 2012).

Figure 4 shows the total shrinkage development of concrete C32-0 measured in the 23^0C and 38^0C rooms for about 6 months. Overall, results show a similar effect of the exposure conditions. The rate of total shrinkage of concrete specimens exposed to the 38^0C environment is higher at early age. However, at long term, the total shrinkage values of concrete exposed to the 23 °C and the 38^0C environments also become similar. The time required for the two shrinkage results to merge is around 50 days (Fig. 4).

It should be noted that the w/b ratio in Table 2 was adjusted to achieve target compressive strength for concrete mixes with different SCM and SCM content. While w/b ratio influences paste volume and hydration kinetics, which can affect shrinkage through changes in capillary porosity and self-desiccation (Lura et al. 2001), its impact in this study was less significant than environmental factors. This is supported by the similar shrinkage values under standard conditions across mixes containing fly ash or slag of the same strength grade, indicating that environmental exposure conditions govern the differences observed in harsh conditions. Previous studies indicated that, for concretes of comparable compressive strength, temperature and RH caused a stronger influence on drying shrinkage than moderate variations in w/b

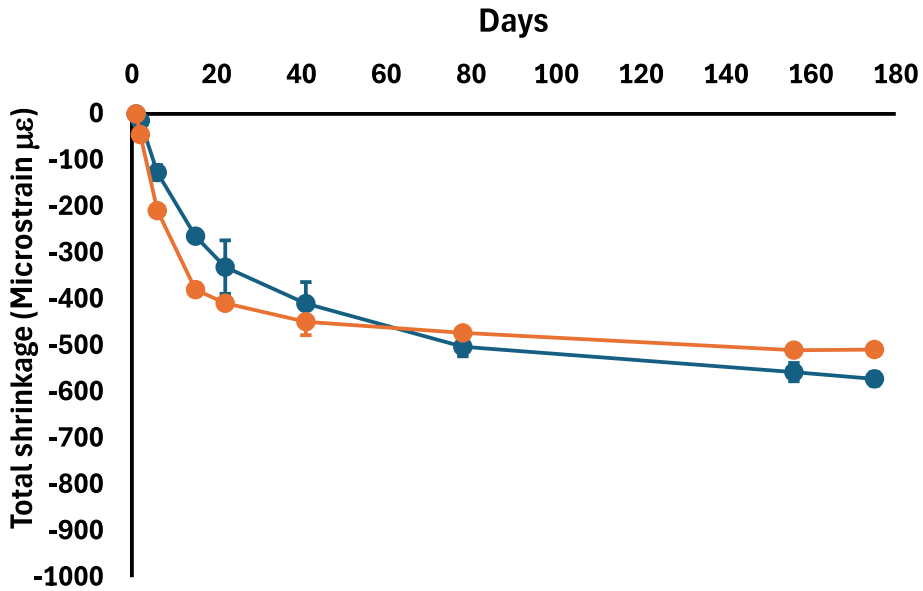

Fig. 4 Total Shrinkage of C32-0 in both 23^0C and 38^0C rooms

ratio (Barluenga et al. 2018; Yalçınkaya and Yazıcı 2017). Therefore, while mix design adjustments may have minor effects, the shrinkage developments reported in this study predominantly reflect environmental influences.

Belabbas et al. (Belabbas et al. 2024) conducted experiments considering 9 different concretes exposed to three different temperatures including 20^0C, 40^0C and 60^0C to investigate the influence of temperature on shrinkage of concrete. Authors reported that increasing the exposure temperature is increasing the total shrinkage of concrete, thus agreeing with this research's findings. In addition, the shrinkage of the concrete specimens exposed to 20^0C and 40^0C stabilised after around 3 months while for the specimens exposed to 60^0C, shrinkage stabilized after around 2 months. In our study, concretes are exposed to 38^0C and the total shrinkage strains tend to stabilize after 50 to 100 days depending on the compressive strength of concrete which is consistent with Belabbas et al. observations.

3.3 Effect of wind on total shrinkage of concrete

Wind speed can considerably increase concrete plastic shrinkage in absence of adequate concrete exposed surface protection (Uno 1998). However, concrete plastic shrinkage is excluded from the scope of this study. This study focuses on hardened concrete shrinkage starting 24 h after casting the specimens. The autogenous shrinkage occurring between concrete setting and 24 h is not accounted for. During this period, drying shrinkage is also prevented by keeping the concrete in sealed moulds. In this study, the effect of the wind speed on the total shrinkage of hardening concrete is investigated by using fans setup in the 38^0C controlled room (Fig. 1). The wind speed produced by the fans was different depending on the concrete specimen distance from the fans and was measured experimentally for each concrete specimen.

Table 4 Wind speed applied on each concrete specimen

Specimen	Wind Speed (km/h)
C32-0–1	21
C32-0–2	18
C32-0–3	13
C45-0–1	22.5
C45-0–2	21.3
C45-0–3	9
C45-FA30-1	20.5
C45-FA30-2	23.6
C45-FA30-3	16.1
C45-G40-1	22.2
C45-G40-2	24.0
C45-G40-3	10.5
C45-G60-1	21.5
C45-G60-2	22.3
C45-G60-3	19.6

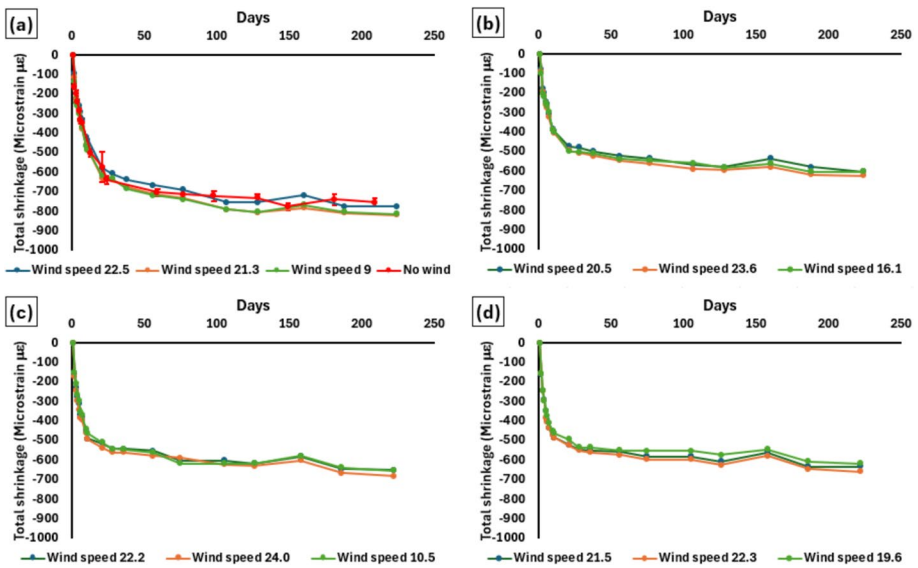

Fig. 5 Effect of wind on total shrinkage of concrete (**a**) C45-0, (**b**) C45-F30, (**c**) C45-G40, (**d**) C45-G60

The wind speed ranged from 9 to 24 kph as shown in Table 4. Only the 45 MPa concretes and C32-0 were tested for wind action.

From Eq. (1), for 38^0C temperature and a relative humidity of 20%, wind speeds ranging from 9 to 24 km/h are leading to water evaporation rates ranging between 2.25 to 2.72 kg/m^2/hr. Therefore, the water evaporation rates will be 6 to 7 times high than that without wind (0.375 kg/m^2/hr). Figure 5 presents the total shrinkage results for concretes C45-0, C45-FA30, C45-G40, C45-G60. Despite the high increase in theoretical water evaporation due to the wind, no significant effect of wind or wind speed on total shrinkage was observed on any of the concrete tested including all binder compositions.

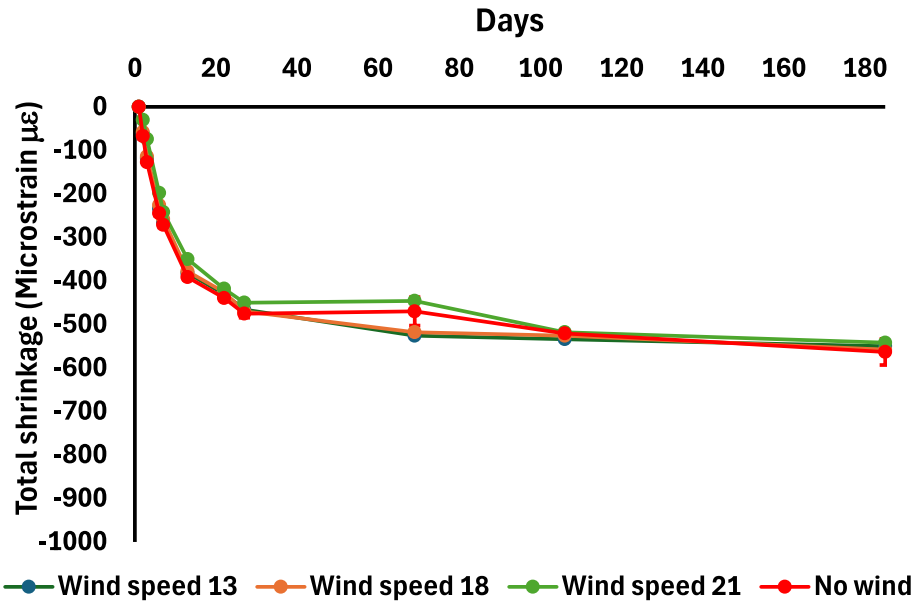

Fig. 6 Effect of wind on total shrinkage of concrete C32-0

Figure 6 presents the total shrinkage results for concretes C32-0. No significant effect of wind or wind speed on total shrinkage was observed for C32-0 either. Results suggest that the wind from the fans contributes to drying the specimen surface but does not influence the internal moisture in the hardened concrete porosity, leading to no increase in drying shrinkage of hardened concrete. Although wind speeds of 9–24 km/h substantially increase the theoretical surface evaporation rate, the drying shrinkage remaining unchanged can be attributed to the strong resistance to internal moisture transport within the concrete matrix. Moisture movement in hardened concrete is governed by diffusion through a highly tortuous and discontinuous pore network, where connectivity and permeability decrease as hydration progresses (Berodier and Scrivener 2015; Cui and Cahyadi 2001; Rahimi-Aghdam et al. 2019). This low diffusivity limits the rate at which internal water can migrate toward the drying surface, even under accelerated evaporation conditions. Moisture transport pathways are primarily through capillary pores and interfacial transition zones, but these become increasingly disconnected as hydration continues, reducing effective diffusivity (Grasley et al. 2006; Meng et al. 2023). In very fine pores less than 7 nm, Knudsen diffusion dominates under low RH conditions, further restricting moisture transport (Zhang et al. 2025). Therefore, even though wind accelerated surface evaporation, the internal moisture redistribution remained diffusion-controlled and slow, preventing significant drying effects into the specimens' core due to the wind.

4 Modelling the effect of water evaporation rate on total shrinkage

The total concrete shrinkage measured in standard conditions is used as the baseline for the model proposed. The model aims to calculate the total shrinkage in harsh conditions, referred in the following as "field conditions". A new time-dependent shrinkage factor, labelled Sh(wer, t) is introduced. Sh(wer, t) is capturing the effect of the water

evaporation rate in the field (wer) calculated using (Eq. 1) excluding the effect of wind in accordance with Sect. 3.3 results. The total shrinkage of concrete exposed to the field conditions is calculated by simply multiplying the total concrete shrinkage measured in standard conditions by Sh(wer, t). The standard conditions considered (23^0C temperature and 50% relative humidity) are the ones used in Australian Standard AS1012.13, which are adopted in most of international standards. The total concrete shrinkage in standard conditions could also be calculated using standard models, such as AS3600 shrinkage model in Australia, selecting interior environment as concrete surface exposure conditions.

Figure 7 shows the time-dependent difference in total shrinkage between the 38^0C room and the 23^0C room for C32-0 and all the 45 MPa concretes. In Fig. 7, the total shrinkage of the specimens exposed to the standard conditions was simply subtracted from the total shrinkage of the specimens exposed to the 38^0C room environment. Overall, the difference in total shrinkage increases until reaching a peak value at a time labelled "peak time" and then decreases until no significant difference can be observed, so called "merging time". For these concretes, the peak time is ranging between 8 and 13 days without showing any clear effect of the binder composition. The average peak time is about 10 days for these concretes. The merging time ranges between 45 to 60 days. The time-dependent increase in strain difference showed in Fig. 7 will be discussed in the next step of the modelling.

Figure 8 shows the time-dependent difference in total shrinkage between the 38^0C room and the 23^0C room for all the 65 MPa concretes. The difference in total shrinkage follows the same trend as for 32 MPa and 45 MPa concretes. The difference in total shrinkage increases until reaching a peak value at peak time and then decreases until no significant difference can be observed, at merging time. The peak time of C65-0 and C65-FA30 concretes is 10 days, which is consistent with the ones observed

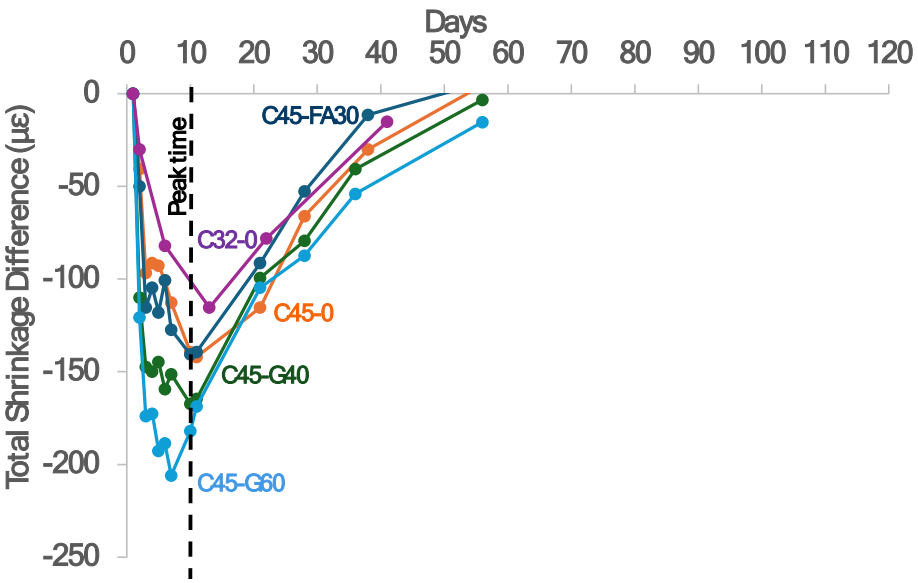

Fig. 7 Time-dependent difference in total shrinkage between the 38^0C room and the 23^0C room for C32-0 and all the 45 MPa concretes

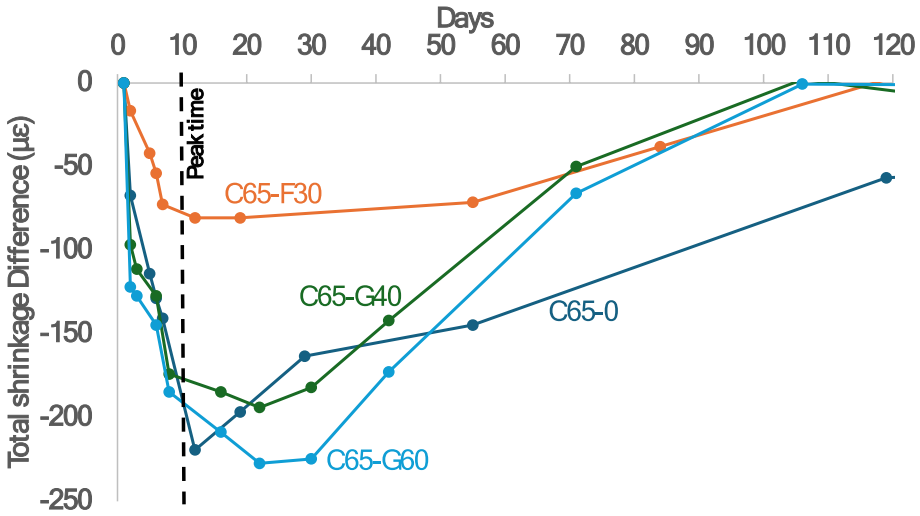

Fig. 8 Time-dependent difference in total shrinkage between the 38^0C room and the 23^0C room for all the 65 MPa concretes

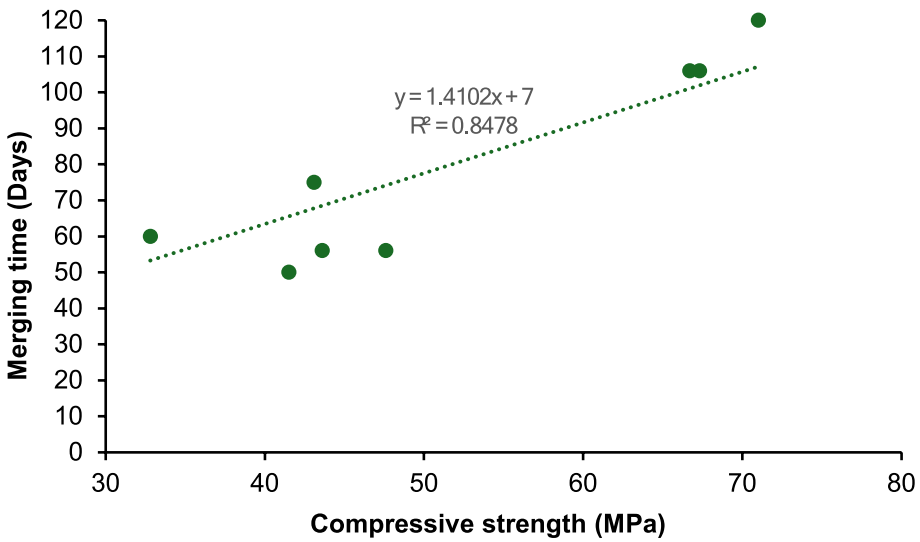

Fig. 9 Relationship between the shrinkage merging time and the 28-day average compressive strength of concretes

for the 32 MPa and 45 MPa concretes. However, the peak time of the two GGBFS concretes appears to increase to about 20 days. Post peak, the reduction in strain difference is not as sharp as for the 32 MPa and 45 MPa concretes. In addition, the merging time of the 65 MPa concretes is consistently over 100 days which is greater than the merging times observed for 32 MPa and 45 MPa concretes. This increase in merging time is consistent with the refined porosity of high strength concrete which requires more time to dry.

Figure 9 shows the relationship between the shrinkage merging time and the 28-day average compressive strength of concretes. C65-0 was excluded because its merging time could not be determined. This concrete is considered as an outlier. According to

Fig. 9 results, for modelling purpose, the shrinkage merging time can be calculated as $1.4f_{cm}+7$ where f_{cm} is the 28-day average concrete compressive strength.

According to the results presented in Figs. 7 and 8, the peak time is close to 10 days or all concretes except C65-G40 and C65-G60, being around 20 days. However, for C65-G40 and C65-G60 concretes, the strain difference at 10 days appears to be close to that at 20 days. It is also clear in Fig. 8 that, post peak, the reduction in strain difference of the 65 MPa concretes is not as sharp as for the 32 MPa and 45 MPa concretes. The strain difference seems closer to a plateau than a sharp peak, sometime for quite a long time, before starting to significantly reduce. To avoid unnecessary complexity in the modelling, a peak time of 10 days is conservatively adopted for all concretes. The delay in strain difference reduction will be managed through other model parameters.

The observed trends of "peak time" and "merging time" used in the development of proposed shrinkage model are closely related to fundamental moisture transport and pore-scale phenomena in concrete. Initially, under harsh conditions (high temperature and low RH), moisture diffusion from the pore network to the surface accelerates due to steep humidity gradients, following a nonlinear Fick's law where diffusivity decreases as internal RH drops (Rahimi-Aghdam et al. 2019; Bažant and Najjar 1971, 1972). Concurrently, internal RH declines both from evaporation-driven drying and self-desiccation during hydration, generating capillary tension in partially saturated pores. This tension, combined with disjoining pressure in nanometer-scale water films, induces contraction of the solid skeleton (Grasley et al. 2006; Beltzung and Wittmann 2005; Rahman and Grasley 2017). These mechanisms explain the rapid increase in shrinkage before "peak time" in harsh environment when moisture gradients and pore suction pressure are at their maximum. As drying and hydration progress, moisture redistribution reduces these gradients, pore pressures diminish, and RH stabilizes, leading to the convergence of shrinkage strains at "merging time". High-strength concretes exhibit longer merging times due to their refined pore structure and lower permeability, which delay internal RH equilibration (Zhang et al. 2014, 2016). Thus, the "peak time" and "merging time" adopted in the model reflect these mechanistic processes, providing a physically consistent basis for predicting shrinkage under varying environmental exposures.

Figures 7 and 8 show the time-dependent total shrinkage difference in microstrains. However, in term of percentage, results show that the increase in shrinkage strain, for all concretes, is fluctuating from 40 to 60% over the period preceding the peak time. An average value of 50% is adopted in the model. As a result, the increase in total shrinkage (compared to standard conditions) is assumed constant and equal to 50% at any time before the peak time. 50% increase is related to the exposure conditions of the 38^0C room with a wer of 0.375 kg/m^2/hr. For wer equal to 0.375, the time-dependent shrinkage factor Sh(0.375, t) is constant and equal to 1.5 before peak time. However, in order to generalise to model to other field exposure conditions, a linear increase versus wer of the time-dependent shrinkage factor during the period preceding the peak time is adopted (Eq. (2)). The first boundary condition is based on the 38^0C room experimental results Sh(0.375, t) = 1.5. The second boundary condition, Sh(0.11, t) = 1, means no increase in total shrinkage if the field wer is equal to the standard exposure condition (wer = 0.11 kg/m^2/hr).

Following the peak time and until the merging time is reached, a non-linear equation is adopted for Sh(wer, t) (Eq. (3)). The effect of the field wer on total shrinkage is reducing exponentially during this period for all concretes. However, the significant effect of the concrete compressive strength on the decrease in shrinkage strain difference and on the merging time (Fig. 9) is taken into account through the coefficient α (Eq. (5)) in the exponential function and the functions K_1 and K_2 in Eq. (3). After reaching the merging time Sh(wer, t) remains constant and equal to 1 (Eq. (4)).

$$\mathrm{Sh(wer,\ t)} = \mathrm{Sh_{wer}} = (-0.5\ \mathrm{wer}\ + 1.5\mathrm{wer_{st}} - 0.375)/(\mathrm{wer_{st}} - 0.375)\ \mathrm{if\ t}\ \leq 10 \quad (2)$$

$$\mathrm{Sh(wer,\ t)}\ =\ \mathrm{K_1}\ +\ \mathrm{K_2}\ \mathrm{e}^{-\alpha \mathrm{t}}\ \mathrm{if\ t}\ >\ 10 \quad (3)$$

$$\mathrm{K_2} = (\mathrm{Sh_{wer}} - 1)/\left(\mathrm{e}^{-10\alpha} - \mathrm{e}^{-(1.4\mathrm{f_{cm}}+7)\alpha}\right)$$

$$\mathrm{K_1} = \mathrm{Sh_{wer}} - \mathrm{K_2 e}^{-10\alpha}$$

$$\mathrm{Sh(wer,\ t)} = 1\ \mathrm{if\ t}\ \geq 1.4\mathrm{f_{cm}} + 7 \quad (4)$$

Where wer is the field water evaporation rate and $\mathrm{wer_{st}}$ is the water evaporation rate is standard conditions ($\mathrm{wer_{st}} = 0.11$).

$$a = -0.0015\mathrm{f_{cm}} + 0.118 \quad (5)$$

Where $\mathrm{f_{cm}}$ is the average 28-day compressive strength of concrete. Figure 10 illustrates the time dependent evolution of Sh(0.375, t) for three compressive strength grades considered in this study. The coefficient α (Eq. 5) was defined as a function of compressive strength because strength serves as a practical and widely accepted input that governs shrinkage behaviour. The compressive strength has been used to predict shrinkage development in several models including fib Model Code, Eurocode 2, Bazant B4 model and Australian Standard AS 3600 (EN 2015; Fib - International Federation for Structural

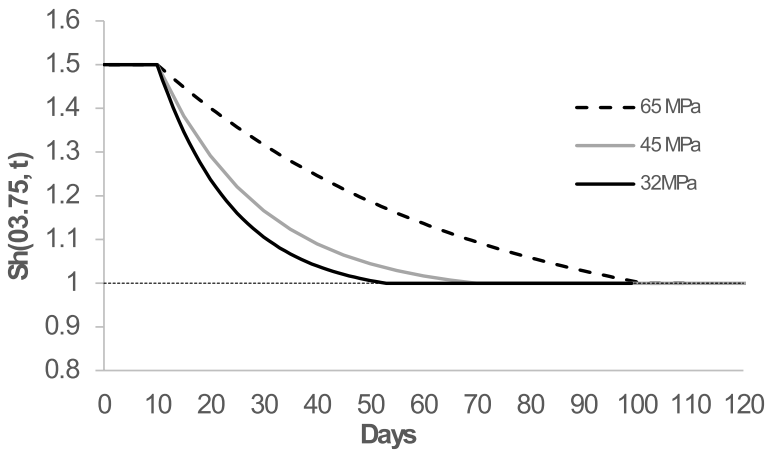

Fig. 10 Time dependent evolution of Sh(0.375, t) for several values of $\mathrm{f_{cm}}$

Concrete 2013; R.T.C 2015; AS 2018). Numerous studies have demonstrated that higher strength concretes exhibit lower porosity, finer pore size distributions, and reduced permeability, all of which slow internal moisture diffusion (Aïtcin 2003). In addition, compressive strength has a high correlation (correlation degree higher than 0.9) with porosity and pore size distribution, making it a reliable indicator of pore refinement (Li et al. 2018; Hou et al. 2019; Jin et al. 2021). Furthermore, hydration rate and water-to-binder ratio, which also affect shrinkage, are inherently reflected in strength development (Berodier and Scrivener 2015; Scrivener et al. 2019). As a result, using compressive strength (f_{cm}) in Eq. (5) as the governing parameter ensures model simplicity and applicability in design practice, where direct measurement of permeability or assessment of pore structure is rarely feasible.

The model parameters were calibrated to fit the experimental results obtained on all concretes tested. The performance of the model is illustrated in Figs. 11, 12, 13, 14 and 15 for concretes C45-F30, C45-G60, C65-G40, C65-0 and C32-0, as examples. Overall, the model predictions of the total shrinkage in the 38^0C room are excellent for all concrete grades and binder compositions considered.

As an example, Fig. 16 shows the effect of different field water evaporation rates (wer) on the model results for the case of C45-FA30. The values of wer are ranging from 0.11 kg/m^2/hr to 0.45 kg/m^2/hr. For wer = 0.11 kg/m^2/hr, $Sh_{wer} = 1$. For wer = 0.25 kg/m^2/hr, $Sh_{wer} = 1.26$. For wer = 0.375 kg/m^2/hr, $Sh_{wer} = 1.5$ and for wer = 0.45 kg/m^2/hr, $Sh_{wer} = 1.64$.

The proposed model was developed and validated using concretes with compressive strengths ranging from 30 to 70 MPa, incorporating fly ash and slag as SCMs, and basalt aggregates. While these conditions represent common structural concretes, the model's applicability to mixtures with different binder chemistries (e.g., limestone calcined clay cement, high-alumina cement), alternative aggregate types,

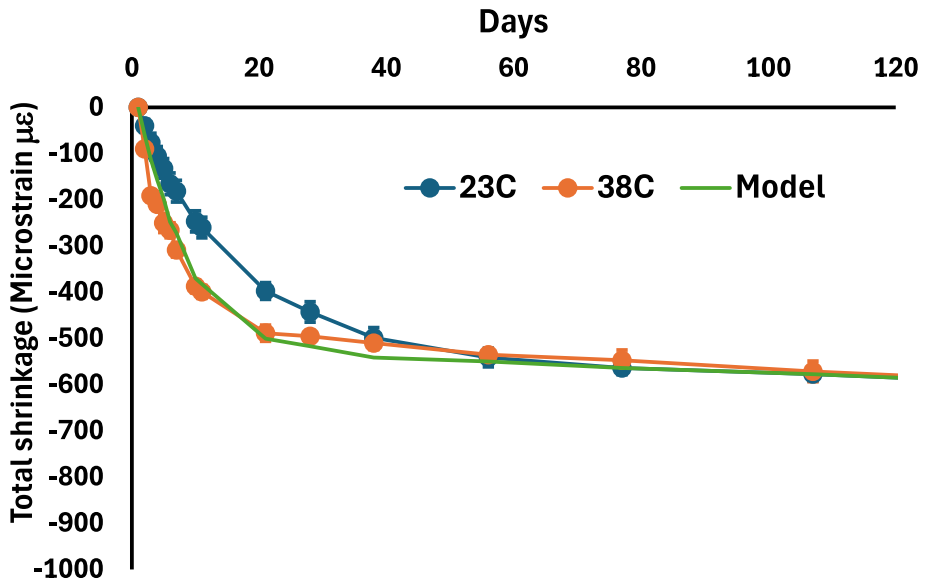

Fig. 11 Model results for C45-F30 concrete total shrinkage in the 38^0C room

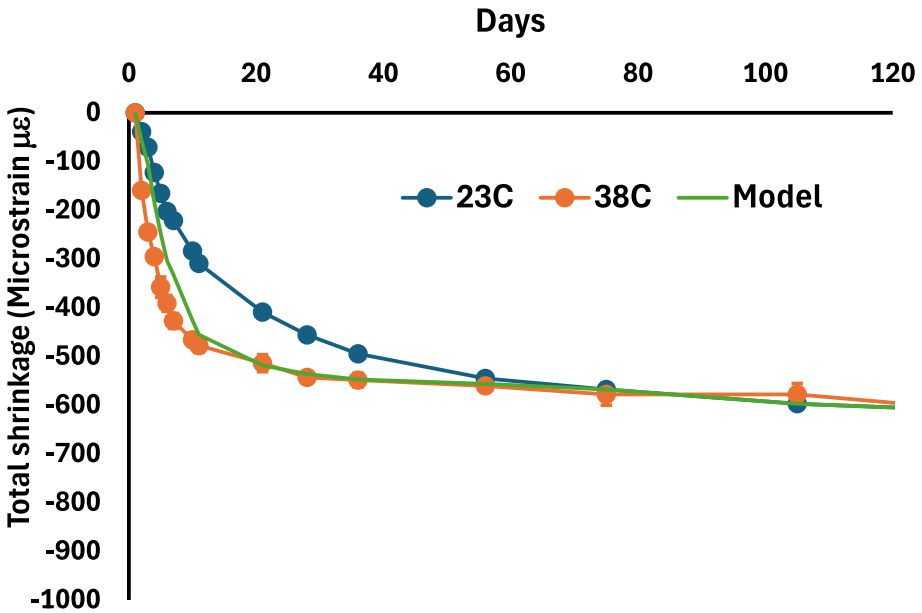

Fig. 12 Model results for C45-G60 concrete total shrinkage in the 38^{0}C room

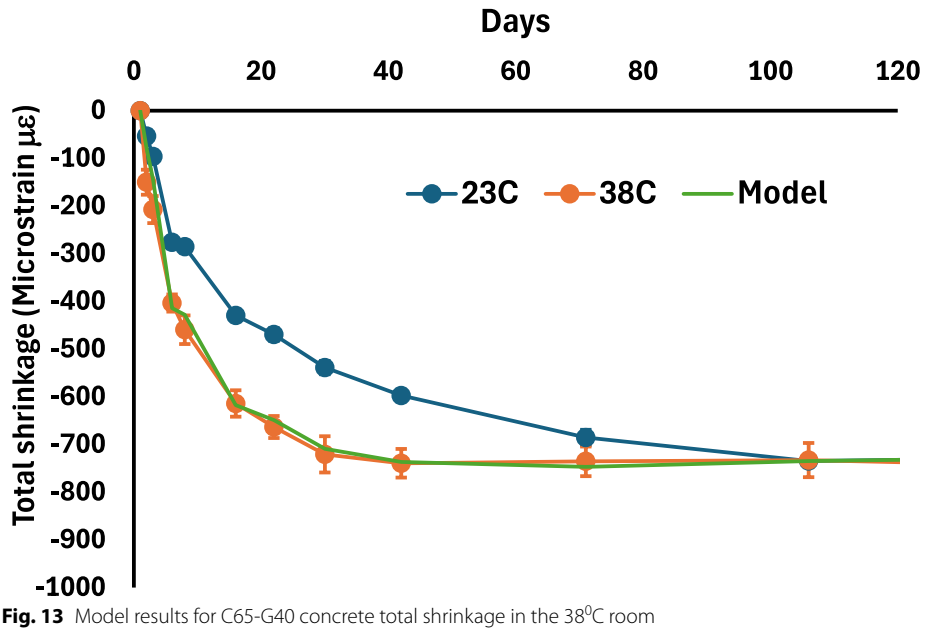

Fig. 13 Model results for C65-G40 concrete total shrinkage in the 38^{0}C room

or concretes containing shrinkage-reducing agents has not been verified. Furthermore, mixtures with very low water-to-binder ratios (w/b less than 0.30), which exhibit high autogenous shrinkage and distinct moisture transport mechanisms, were outside the scope of this study. Future works are required to investigate these variables to refine the model and ensure broader applicability across diverse concrete compositions and environmental conditions.

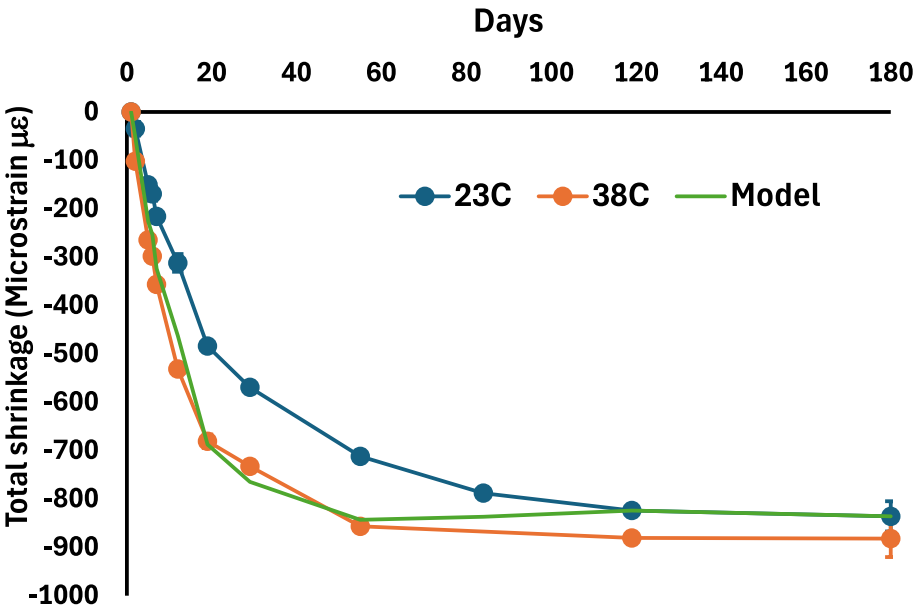

Fig. 14 Model results for C65-0 concrete total shrinkage in the 38^0C room

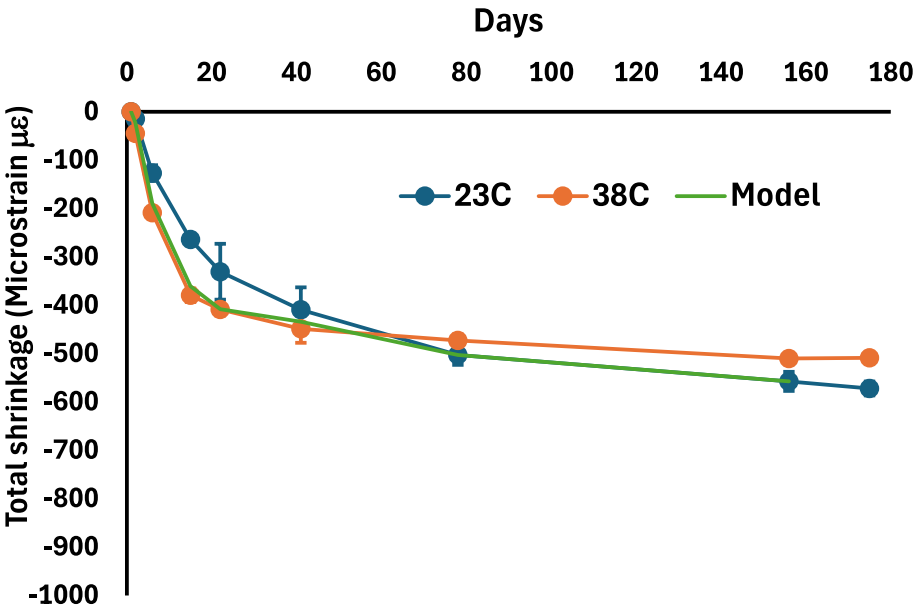

Fig. 15 Model results for C32-0 concrete total shrinkage in the 38^0C room

5 Conclusions

This paper is proposing a new model aiming to calculate the concrete total shrinkage in harsh conditions, referred as "field conditions", from the concrete total shrinkage measured or calculated in standard conditions (23^0C temperature and 50% relative humidity). A new time-dependent shrinkage factor, labelled Sh(wer, t) is introduced. The total shrinkage of concrete exposed to the field conditions is calculated by simply multiplying the total concrete shrinkage in standard conditions by Sh(wer, t).

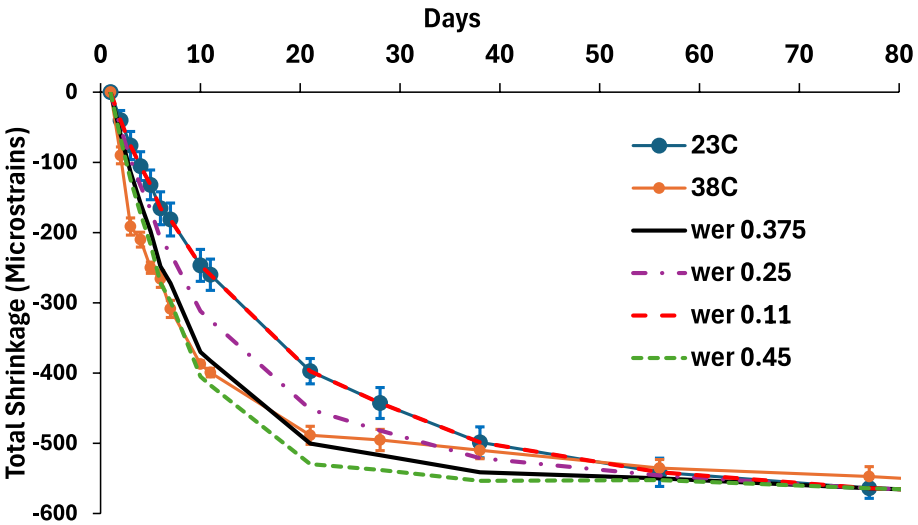

Fig. 16 Effect of different field water evaporation rate (wer) on the model results for the case of C45-FA30

Experimental results showed that wind action has no significant effect on the total shrinkage of hardened concrete. Plastic shrinkage was not part of this investigation. Results suggest that the wind contributes to drying the specimen surface but does not influence the internal moisture in the hardened concrete porosity. As a result, the effect of wind speed is not accounted for in the calculation of the field water evaporation rate. The field water evaporation rate is calculated from the assumed field temperature and relative humidity.

The increase in total shrinkage between standard conditions and harsh field conditions was similar in trend for all concretes. Total shrinkage in harsh conditions increases until reaching a peak value and then decreases until no significant difference can be observed, at the so-called merging time. This trend was only marginally dependent on the concrete binder composition. However, the post peak phase was significantly dependent on the concrete compressive strength. The merging time greatly increases with an increase in concrete compressive strength.

Overall, the model predictions of the total shrinkage in harsh field exposure conditions are excellent for concrete compressive strengths ranging from about 30 MPa to 70 MPa, including 100% general purpose cement concretes and fly ash and slag blended cement-based concretes.

Acknowledgements
We also acknowledge University of Technology Sydney's supports and laboratories technician from civil lab for their supports.

Authors' contributions
Htet Nyi Nyi Lin: Writing – original draft, Visualization, Software, Methodology, Investigation, Formal analysis, Data curation, Conceptualization. Quang Dieu Nguyen: Writing – review & editing, Writing – original draft, Visualization, Resources, Project administration, Methodology, Investigation, Formal analysis, Data curation, Conceptualization. Arnaud Castel: Writing – review & editing, Writing – original draft, Supervision, Resources, Project administration, Funding acquisition, Conceptualization.

Funding
This work was supported by a research grant titled "Refining Design Deformation Predictions by Improving Concrete Volume Stability Assessment (22.PP.0151)" from SmartcreteCRC and BG&E Consulting Engineers. The content of this paper reflects the views of the authors, who are responsible for the facts and the accuracy of the data presented herein and does not necessarily reflects the official view of SmartcreteCRC and BG&E Consulting Engineers.

Data availability
Data will be made available on request.

Declarations

Competing interests
The authors declare that they have no known competing financial interests or personal relationships that could have appeared to influence the work reported in this paper.

Received: 4 November 2025 Revised: 11 December 2025 Accepted: 1 January 2026
Published online: 05 April 2026

References

Afroz S, Nguyen QD, Zhang Y, Kim T, Castel A (2022) Evaluation of cracking potential parameters for low to high grade concrete with fly ash or slag. Constr Build Mater 350:128891
Afroz S, Zhang Y, Nguyen QD, Kim T, Castel A (2023) Shrinkage of blended cement concrete with fly ash or limestone calcined clay. Mater Struct 56:15
Aïtcin PC (2003) The durability characteristics of high performance concrete: a review. Cem Concr Compos 25:409–420
AS, AS 3972: General purpose and blended cements, Standards Australia, Sydney, Australia, 2010
AS, AS 3600: Concrete structures, Standards Australia, Sydney, Australia, 2018
Asamoto S, Kurashige I, Chun P-J (2023) Effect of high temperature at early ages on drying shrinkage and creep of concrete focusing on microcracking damage. Mater Struct 56:67
ASTM, ASTM C39/C39M-18: Standard Test Method for Compressive Strength of Cylindrical Concrete Specimens, ASTM International, West Conshohocken, PA, 2018
Atiş CD (2003) High-volume fly ash concrete with high strength and low drying shrinkage. J Mater Civ Eng 15:153–156
Aziz W, Aslam M, Ejaz M.F, Jahanzaib M, Ali, R. Ahmad, M. Wajeeh-ul-Hassan Raza, A. Khan, Mechanical properties, drying shrinkage and structural performance of coconut shell lightweight concrete. Structures. 35 (2022) 26–35
Barluenga G, Guardia C, Puentes J (2018) Effect of curing temperature and relative humidity on early age and hardened properties of SCC. Constr Build Mater 167:235–242
Bažant ZP, Najjar LJ (1971) Drying of concrete as a nonlinear diffusion problem. Cem Concr Res 1:461–473
Bažant ZP, Najjar LJ (1972) Nonlinear water diffusion in nonsaturated concrete. Mater Struct 5:3–20
Belabbas O, Bouziadi F, Boulekbache B, Hamrat M, Haddi A, Amziane S (2024) Mechanical properties of multi-recycled coarse aggregate concrete, with particular emphasis on experimental and numerical assessment of shrinkage at different curing temperatures. J Build Eng 89:109333
Beltzung F, Wittmann FH (2005) Role of disjoining pressure in cement based materials. Cem Concr Res 35:2364–2370
Berodier E, Scrivener K (2015) Evolution of pore structure in blended systems. Cem Concr Res 73:25–35
Bisht K, Ramana PV (2022) Experimental investigation of strength, drying shrinkage, freeze and thaw and fire attack properties of concrete mixes with beverage glass waste as fine aggregate. Struct 36:358–371
Brooks JJ, Johari MAM (2001) Effect of metakaolin on creep and shrinkage of concrete. Cem Concr Compos 23:495–502
Choudhary R, Gupta R, Alomayri T, Jain A, Nagar R (2021) Permeation, corrosion, and drying shrinkage assessment of self-compacting high strength concrete comprising waste marble slurry and fly ash, with silica fume. Struct 33:971–985
Chu I, Kwon SH, Amin MN, Kim J-K (2012) Estimation of temperature effects on autogenous shrinkage of concrete by a new prediction model. Constr Build Mater 35:171–182
Cui L, Cahyadi JH (2001) Permeability and pore structure of OPC paste. Cem Concr Res 31:277–282
Dellinghausen LM, Gastaldini ALG, Vanzin FJ, Veiga KK (2012) Total shrinkage, oxygen permeability, and chloride ion penetration in concrete made with white Portland cement and blast-furnace slag. Constr Build Mater 37:652–659
Dhahir MK, Marx S (2024) Shrinkage behaviour of high-strength concrete plates reinforced with carbon textile reinforcement. Structures 69:107504
EN 1992–1–1: Eurocode 2: Design of concrete structures, Part 1–1: General rules and rules for buildings, European Standard, Brussels, 2015
Fib - International Federation for Structural Concrete (2013) Fib model code for concrete structures 2010. Wilhelm Ernst & Sohn, Berlin, Germany
Gedam BA, Bhandari NM, Upadhyay A (2016) Influence of supplementary cementitious materials on shrinkage, creep, and durability of high-performance concrete. J Mater Civ Eng 28:04015173
Giergiczny Z (2019) Fly ash and slag. Cem Concr Res 124:105826
Gilbert RI, Ranzi G (2010) Time-dependent behaviour of concrete structures. CRC Press, London
Gilbert RI, Bradford MA, Gholamhoseini A, Chang ZT (2012) Effects of shrinkage on the long-term stresses and deformations of composite concrete slabs. Eng Struct 40:9–19
Grasley ZC, Lange DA, D'Ambrosia MD (2006) Internal relative humidity and drying stress gradients in concrete. Mater Struct 39:901–909
Hou D, Li D, Hua P, Jiang J, Zhang G (2019) Statistical modelling of compressive strength controlled by porosity and pore size distribution for cementitious materials. Cem Concr Compos 96:11–20
Hui Q, Yan L, Zhang Z, Wang A (2024) Shrinkage and creep effect analysis of beam-arch composite bridge based on field test. Structures 62:106187
Jin L, Yu W, Du X, Yang W (2020) Meso-scale simulations of size effect on concrete dynamic splitting tensile strength: influence of aggregate content and maximum aggregate size. Eng Fract Mech 230:106979

Jin S, Zhou J, Zhao X, Sun L (2021) Quantitative relationship between pore size distribution and compressive strength of cementitious materials. Constr Build Mater 273:121727
John VM, Quattrone M, Abrão PCRA, Cardoso FA (2019) Rethinking cement standards: opportunities for a better future. Cem Concr Res 124:105832
Li D, Li Z, Lv C, Zhang G, Yin Y (2018) A predictive model of the effective tensile and compressive strengths of concrete considering porosity and pore size. Constr Build Mater 170:520–526
Lura P, Van Breugel K, Maruyama I (2001) Effect of curing temperature and type of cement on early-age shrinkage of high-performance concrete. Cem Concr Res 31:1867–1872
Ma HC, Geng Y, Wang QH, Lai LH, Li GD, Wang YY (2025) Autogenous shrinkage model for concrete with weathered steel slag coarse aggregate. Structures 75:108862
Meng Z, Zhang Y, Chen WK, Fu CQ, Xiong QX, Zhang CL, Liu QF (2023) A numerical study of moisture and ionic transport in unsaturated concrete by considering multi-ions coupling effect. Transp Porous Media 151:339–366
S.L. Meyers, Thermal expansion characteristics of hardened cement paste and of concrete, 1951
Nguyen QD, Afroz S, Zhang Y, Kim T, Li W, Castel A (2022) Autogenous and total shrinkage of limestone calcined clay cement (LC3) concretes. Constr Build Mater 314:125720
Piasta W, Zarzycki B (2017) The effect of cement paste volume and w/c ratio on shrinkage strain, water absorption and compressive strength of high performance concrete. Constr Build Mater 140:395–402
R.T.C. TC-242-MDC, (2015) RILEM draft recommendation: TC-242-MDC multi-decade creep and shrinkage of concrete: material model and structural analysis*, Materials and Structures, 48:753–770.
Rahimi-Aghdam S, Rasoolinejad M, Bažant ZP (2019) Moisture diffusion in unsaturated self-desiccating concrete with humidity-dependent permeability and nonlinear sorption isotherm. J Eng Mech 145:04019032
Rahman SF, Grasley ZC (2017) The significance of pore liquid pressure and disjoining pressure on the desiccation shrinkage of cementitious materials. Int J Adv Eng Sci Appl Math 9:87–96
Sakata K, Ayano T (2000) Effect of ambient temperature and humidity on creep and shrinkage of concrete. ACI Special Publication, American Concrete Institute, pp 215–235
Scrivener K, Ouzia A, Juilland P, Kunhi Mohamed A (2019) Advances in understanding cement hydration mechanisms. Cem Concr Res 124:105823
Snellings R, Mertens G, Elsen J (2012) Supplementary cementitious materials. Rev Mineral Geochem 74:211–278
Uno PJ (1998) Plastic shrinkage cracking and evaporation formulas. ACI Mater J 95:365–375
Yalçınkaya Ç, Yazıcı H (2017) Effects of ambient temperature and relative humidity on early-age shrinkage of UHPC with high-volume mineral admixtures. Constr Build Mater 144:252–259
Zhang W, Zakaria M, Hama Y (2013) Influence of aggregate materials characteristics on the drying shrinkage properties of mortar and concrete. Constr Build Mater 49:500–510
Zhang J, Han YD, Gao Y (2014) Effects of water-binder ratio and coarse aggregate content on interior humidity, autogenous shrinkage, and drying shrinkage of concrete. J Mater Civ Eng 26:184–189
Zhang J, Han Y, Zhang J (2016) Evaluation of shrinkage induced cracking in concrete with impact of internal curing and water to cement ratio. J Adv Concr Technol 14:324–334
Zhang Y, Afroz S, Nguyen QD, Kim T, Nguyen D, Castel A, Nairn J, Gilbert RI (2023a) Autogenous shrinkage of fly ash and ground granulated blast furnace slag concrete. Mag Concr Res 75:283–295
Zhang Y, Kim T, Castel A, Xu T (2023b) Thermal cracking in high volume of fly ash and GGBFS concrete. Int J Concr Struct Mater 17:65
Zhang X, S. Zhang, B. Chen, B. Tian, X. Lu, B. Xiong, Z. Pan, Study of Concrete Moisture Transfer Characteristics in the Presence of the Concrete Micro–Meso Structure Effect, Applied Sciences, 2025, pp. 1774

Publisher's Note